Mathematical and Computational Applications

MDPI

Article

Numerical Solution of Natural Convection Problems Using Radial Point Interpolation Meshless (RPIM) Method Combined with Artificial-Compressibility Model

Pranowo [1,2], Albertus Joko Santoso [1] and Agung Tri Wijayanta [2,3,*]

[1] Department of Informatics, Universitas Atma Jaya Yogyakarta, Jl. Babarsari 44, Yogyakarta 55281, Indonesia; pranowo@uajy.ac.id (P.); joko.santoso@uajy.ac.id (A.J.S.)
[2] Research Group of Sustainable Thermofluids, Faculty of Engineering, Universitas Sebelas Maret, Jl. Ir. Sutami 36A Kentingan, Surakarta 57126, Indonesia
[3] Department of Mechanical Engineering, Faculty of Engineering, Universitas Sebelas Maret, Jl. Ir. Sutami 36A Kentingan, Surakarta 57126, Indonesia
* Correspondence: agungtw@uns.ac.id

Abstract: A numerical method is used to solve the thermal analysis of natural convection in enclosures. This paper proposes the use of an implicit artificial-compressibility model in conjunction with the Radial Point Interpolation Meshless (RPIM) method to mimic laminar natural convective heat transport. The technique couples the pressure with the velocity components using an artificial compressibility model. The RPIM is used to discretize the spatial terms of the governing equation. We solve the semi-algebraic system implicitly in backward Euler pseudo-time. The proposed method solves two test problems—natural convection in the annulus of concentric circular cylinders and trapezoidal cavity. Additionally, the results are validated using experimental and numerical data available in the literature. Excellent agreement was seen between the numerical results acquired with the suggested method and those obtained through the standard techniques found in the literature.

Keywords: natural convection; annulus; trapezoidal; meshless method; artificial compressibility

check for updates

Citation: Pranowo; Santoso, A.J.; Wijayanta, A.T. Numerical Solution of Natural Convection Problems Using Radial Point Interpolation Meshless (RPIM) Method Combined with Artificial-Compressibility Model. *Math. Comput. Appl.* **2024**, *29*, 39. https://doi.org/10.3390/mca29030039

Academic Editor: Zhuojia Fu

Received: 10 April 2024
Revised: 12 May 2024
Accepted: 15 May 2024
Published: 20 May 2024

Copyright: © 2024 by the authors. Licensee MDPI, Basel, Switzerland. This article is an open access article distributed under the terms and conditions of the Creative Commons Attribution (CC BY) license (https://creativecommons.org/licenses/by/4.0/).

1. Introduction

Nowadays, the development of meshless methods for numerical modeling, especially heat transfer by natural convection, has attracted much attention from researchers. This method is flexible because it does not require a mesh so that any domain shape can be modeled. Coordinate points spread across the space domain are needed as a substitute for a mesh, so this method is much simpler than methods that require a mesh, such as the Finite Element, Finite Volume, Finite Difference, and Lattice Boltzmann methods [1,2]. Sadat and Couturier [3] developed a meshless method called the Diffuse Approximation Method (DAM) for modeling natural convection. Sophy et al. [4] successfully developed this method for modeling three-dimensional convection. At almost the same time, Liu and Wu [5] developed a meshless method called the Point Interpolation Method (PIM); this method uses low-order polynomial approximations such as the DAM method. The results of this method were proven to be suitable only for calculations with low Rayleigh Numbers. Wijayanta and Pranowo [6] used a localized meshless with Radial Basis Function (RBF) as the interpolation function; the calculation results showed this method's high accuracy.

The method above solves the model equation in "strong form"; this approach is entirely accurate but sensitive to changes in numerical parameters, so it is less robust. Several researchers proposed solving the model equation in "weak form" by integrating it according to the Galerkin procedure. This method was adopted from the Finite Element method (FEM). The weak-form meshless method was initially successfully developed by Belytschko et al. [7,8] for solid mechanics modeling, especially for calculating crack

propagation. This method is called element-free Galerkin (EFG), which received much attention from researchers and was developed to solve various problems in the engineering field. Manzin and Bottauscio [9] used the EFG method to calculate the scattering of electromagnetic waves in a non-homogeneous medium. Singh et al. [10] expanded the use of the EFG method for calculating nonlinear conduction heat transfer. The use of the EFG method for numerical calculations of fluid mechanics was carried out by Singh and Jain [9]; they developed a parallel algorithm for the numerical solution of the Steady Navier–Stokes Equations without involving convection terms. Vlastelica et al. [11] explored the use of the EFG method for numerical calculations of incompressible viscous fluid flows. They observed the effect of the number of integration points on the accuracy of the EFG method.

The development of the EFG method continues to be carried out significantly to increase its accuracy; Zhang et al. [12–14] developed the multiscale EFG method. This method divides the numerical solution into two parts, namely the global level solution and the local level solution. Local-level solutions help increase accuracy, especially in parts of the domain that contain sharp gradients. This method has been successfully used to calculate numerical solutions to the Stokes equation [12], incompressible fluid flow [11], and heat transfer by natural convection in complex-shaped domains [12].

Recently, some fluid flow and heat convection issues have been taken into account by the meshless local Petrov–Galerkin (MLPG) approach. The MLPG method was successfully developed to simulate incompressible fluid flow using the stream function-vorticity formulation [15–17]. However, this formulation is difficult to apply to complex geometric shapes because the boundary conditions for the flow function and vorticity at the wall are difficult to determine. Apart from that, this method also cannot solve three-dimensional problems. Efforts to solve incompressible fluid flow using primitive variables were pioneered by Atluri and colleagues [18,19]. Najafi et al. [20,21] succeeded in further developing the MLPG method based on primitive variables for convection heat transfer problems.

The main weakness of the EFG method is that the Dirichlet boundary conditions are difficult to apply directly because the interpolation function uses a least square error approach with low-order polynomial interpolation. Applying Dirichlet boundary conditions requires using the Lagrange Multiplier approach, so the results are not exact. Based on the description above, this research proposes using a meshless numerical method with a "weak form" approach and basis functions using RBF for modeling natural convection in porous media and air. Using RBF basis functions makes it easier to implement Dirichlet boundary conditions. This method is called the Radial Point Interpolation Meshless (RPIM) method [22].

2. The Governing Equations

The model equations used are the two-dimensional Navier–Stokes and energy conservation equations. If the temperature differences that occur are small, then the Boussinesq approach is applicable for modeling the buoyancy force. Thus, the two-dimensional Navier–Stokes equations and energy equations can be written as follows [23]:

$$\frac{\partial u}{\partial x} + \frac{\partial v}{\partial y} = 0 \tag{1}$$

$$\frac{\partial u}{\partial t} + u\frac{\partial u}{\partial x} + v\frac{\partial u}{\partial y} = -\frac{\partial p}{\partial x} + \frac{Pr}{Ra^{0.5}}\left(\frac{\partial^2 u}{\partial x^2} + \frac{\partial^2 u}{\partial y^2}\right) \tag{2}$$

$$\frac{\partial v}{\partial t} + u\frac{\partial v}{\partial x} + v\frac{\partial v}{\partial y} = -\frac{\partial p}{\partial y} + \frac{Pr}{Ra^{0.5}}\left(\frac{\partial^2 v}{\partial x^2} + \frac{\partial^2 v}{\partial y^2}\right) + Pr\theta \tag{3}$$

$$\frac{\partial \theta}{\partial t} + u\frac{\partial \theta}{\partial x} + v\frac{\partial \theta}{\partial y} = \frac{1}{Ra^{0.5}}\left(\frac{\partial^2 \theta}{\partial x^2} + \frac{\partial^2 \theta}{\partial y^2}\right) \tag{4}$$

where the two-dimensional spatial coordinates are (x,y), the time is t, the pressure is p, the temperature is θ, and the velocity components are (u,v). The dimensionless equations

are obtained by dividing dimension variables with the reference variables. The reference variable for length is $L_r = H$, for velocity $V_r = (\alpha/H)\, Ra^{0.5}$, for the time $t_r = (H^2/\alpha)\, Ra^{-0.5}$, for the temperature ($\theta$) is defined as follows: $(T - T_c)/(T_h - T)_c$.

3. The Radial Point Interpolation Meshless (RPIM) Method

This section briefly introduces the RPIM approximation for function $u(\mathbf{x})$ utilizing just nodal function value (u_i) at a collection of local nodes. Let $\mathbf{x}_i$ be a set of randomly distributed points in a domain (i = 1, 2,..., n), where n is the number of nodes in the support domain. The expression for the function $u(\mathbf{x})$ approximation can be written as follows [22,24]:

$$u(\mathbf{x}) = \sum_{i=1}^{n} \phi_i u_i \tag{5}$$

The above equation becomes:

$$u(\mathbf{x}) = \boldsymbol{\varphi}(\mathbf{x})\mathbf{U_s} \tag{6}$$

$$\boldsymbol{\varphi}(\mathbf{x}) = \mathbf{R}_\mathbf{Q}^T(\mathbf{x})\mathbf{R}_\mathbf{Q}^{-\mathbf{1}}(\mathbf{x}_i) \tag{7}$$

when expressed in matrix form.

$$\mathbf{x}^T = [x, y] \tag{8}$$

$$\mathbf{U_s} = [u_1, u_2, u_3, \ldots, u_n]^T \tag{9}$$

$$\mathbf{R_Q}(\mathbf{x}_i) = \begin{bmatrix} R_1(\mathbf{x}_1) & R_2(\mathbf{x}_1) & \ldots & R_n(\mathbf{x}_1) \\ R_1(\mathbf{x}_2) & R_2(\mathbf{x}_2) & \ldots & R_n(\mathbf{x}_2) \\ \ldots & \ldots & \ldots & \ldots \\ R_1(\mathbf{x}_n) & R_2(\mathbf{x}_n) & \ldots & R_n(\mathbf{x}_n) \end{bmatrix} \tag{10}$$

Whereas **R** is the matrix holding the radial basis function (RBF) interpolation, $\mathbf{U_s}$ is the vector containing the value u at the node point (Figure 1). The vector **x** represents spatial coordinates. The function chosen for interpolation is the multiquadric RBF function:

$$R_i(x, y) = \left(r_i^2 + C^2\right)^{0.5} = \left[(x - x_i)^2 + (y - y_i)^2 + C^2\right]^{0.5} \tag{11}$$

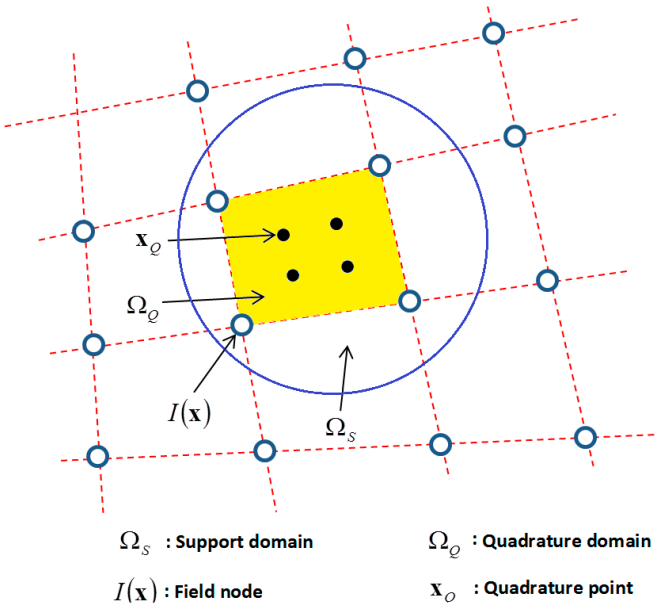

Figure 1. Support domain and quadrature domain.

The constants C are the shape parameters.

In Equation (6), $\boldsymbol{\varphi}(\mathbf{x})$ is RPIM shape functions corresponding to the nodal value and given by

$$\boldsymbol{\varphi}(\mathbf{x}) = [\phi_1(\mathbf{x}), \phi_2(\mathbf{x}), \phi_3(\mathbf{x}), \ldots, \phi_n(\mathbf{x})]^T \tag{12}$$

in which

$$\phi_k(\mathbf{x}) = \sum_{i=1}^{n} R_i(\mathbf{x}) G_{(i,k)} \tag{13}$$

where $G_{(i,k)}$ is the element of matrix $\mathbf{R_Q^{-1}}$.

After the shape functions are determined, the shape function derivatives can be calculated as follows:

$$\begin{array}{l} \frac{\partial \phi_k}{\partial x}(\mathbf{x}) = \sum\limits_{i=1}^{n} \frac{\partial R_i}{\partial x}(\mathbf{x}) G_{(i,k)} \\ \frac{\partial \phi_k}{\partial y}(\mathbf{x}) = \sum\limits_{i=1}^{n} \frac{\partial R_i}{\partial y}(\mathbf{x}) G_{(i,k)} \end{array} \tag{14}$$

Similar expressions can be used for the primitive variables in the model equations (u,v,p,θ):

$$\begin{array}{l} u(\mathbf{x}) = \sum\limits_{i=1}^{n} \phi_i u_i \; ; v(\mathbf{x}) = \sum\limits_{i=1}^{n} \phi_i v_i \\ p(\mathbf{x}) = \sum\limits_{i=1}^{n} \phi_i p_i \; ; \theta(\mathbf{x}) = \sum\limits_{i=1}^{n} \phi_i \theta_i \end{array} \tag{15}$$

The RPIM method still requires a mesh background for spatial integration with the Gauss quadrature method, so this method is not a pure meshless method. The shape of the elements in the background mesh can be arbitrary as long as Gauss quadrature integration can be carried out. This study chose the background mesh as a quadrilateral quadrature domain because it is simple (Figure 1).

After the compact support and quadrature domains are determined, the next step is to carry out Galerkin integration using a weight function equal to the shape function. Equation (4) is used as an example of integration:

$$\int_{\Omega_Q} \phi_i \left(\frac{\partial \theta}{\partial t} + u \frac{\partial \theta}{\partial x} + v \frac{\partial \theta}{\partial y} - \frac{1}{Ra^{0.5}} \left(\frac{\partial^2 \theta}{\partial x^2} + \frac{\partial^2 \theta}{\partial y^2} \right) \right) d\Omega = 0 \tag{16}$$

Substitute the temperature expansion (Equation (14)) into Equation (15):

$$M_{ij} \frac{\partial \theta_j}{\partial t} + C_{ij} \theta_j + \frac{1}{Ra^{0.5}} K_{ij} \theta_j = 0 \tag{17}$$

$$M_{ij} = \int_{\Omega_Q} \phi_i \phi_j d\Omega \tag{18}$$

$$C_{ij} = \int_{\Omega_Q} \phi_i \left(u_j \frac{\partial \phi_j}{\partial x} + v_j \frac{\partial \phi_j}{\partial y} \right) d\Omega \tag{19}$$

$$K_{ij} = \int_{\Omega_Q} \left(\frac{\partial \phi_i}{\partial x} \frac{\partial \phi_j}{\partial x} + \frac{\partial \phi_i}{\partial y} \frac{\partial \phi_j}{\partial y} \right) d\Omega \tag{20}$$

Equation (17) is a global semi-algebraic equation. All spatial integration calculation matrices are carried out using the Galerkin procedure in each support domain and then assembled into a global semi-algebraic equation (Equation (17)).

The discretization of Equations (2) and (3) is carried out in the same way; the results are as follows:

$$M_{ij}\frac{\partial u_j}{\partial t} + C_{ij}u_j + \frac{Pr}{Ra^{0.5}}K_{ij}u_j - D^x{}_{ij}p_i = 0$$

$$M_{ij}\frac{\partial v_j}{\partial t} + C_{ij}v_j + \frac{Pr}{Ra^{0.5}}K_{ij}v_j - D^y{}_{ij}p_i - PrM_{ij}\theta_j = 0$$

The main difficulty in solving the incompressible flow equation is due to the pressure being decoupled from the velocity field. Chorin proposed the artificial compressibility method to alleviate this problem [25]. Due to their ease of use and effectiveness, the artificial compressibility for incompressible flows has been widely used by numerous researchers [26–29]. The pressure field is linked to Equation (1) in the following way using the artificial compressibility method:

$$\frac{\partial p}{\partial t} + \beta\left(\frac{\partial u}{\partial x} + \frac{\partial v}{\partial y}\right) = 0 \tag{21}$$

The derivative of pressure over time in the equation above is a pseudo-variable because the equation above actually only applies to compressible flow. Thus, the transient solution of the system of equations has no physical meaning; only the steady state has physical meaning. Meanwhile, β is an artificial compressibility factor whose value is constant. The β constant is equivalent to the square of the sound speed of the medium, so in this paper, the β is 10^6.

Discretization of the RPIM method for Equation (19) produces the discrete equation:

$$M_{ij}\frac{\partial p_j}{\partial t} + \beta\left(D^x{}_{ij}u_j + D^y{}_{ij}v_j\right) = 0 \tag{22}$$

Time integration of the semi-algebraic equations is carried out using the implicit Euler method so that the calculations are stable:

$$\begin{bmatrix} M_{ij} & \Delta t\beta D^x{}_{ij} & \Delta t\beta D^y{}_{ij} & 0 \\ -\Delta t D^x{}_{ij} & A_{ij} + \frac{Pr}{Ra^{0.5}}\Delta t K_{ij} & 0 & -\Delta t M_{ij} Pr \\ -\Delta t D^x{}_{ij} & 0 & A_{ij} + \frac{Pr}{Ra^{0.5}}\Delta t K_{ij} & 0 \\ 0 & 0 & 0 & A_{ij} + \frac{1}{Ra^{0.5}}\Delta t K_{ij} \end{bmatrix} \begin{bmatrix} p_j^{n+1} \\ u_j^{n+1} \\ v_j^{n+1} \\ \theta_j^{n+1} \end{bmatrix} = \begin{bmatrix} M_{ij}p_j^n \\ M_{ij}u_j^n \\ M_{ij}v_j^n \\ M_{ij}\theta_j^n \end{bmatrix} \tag{23}$$

$$A_{ij} = M_{ij} + \Delta t C_{ij} \tag{24}$$

The RPIM algorithm for solving natural convection problems is described as follows [30]:

1. Specify maximum pseudo-time for the calculation and time step, the initial condition, boundary condition, primitive variables (u, v, p, θ), node coordinates, basis function parameters, background mesh, Support domain and quadrature domain.
2. Calculate the derivative operator matrices in Equations (17)–(20).
3. Pseudo-time marching starts.
4. Calculate the global matrix and the right side vector in Equation (2).
5. Solve the global matrix to obtain the primitive variables $(u, v, p, \theta)^{n+1}$
6. Update the pseudo time $(n + 1)$.
7. Check if it has reached the maximum time limit, if not back to step 2. If it is go to step 8.
8. Finish.

4. Results and Discussion

In the framework of the artificial-compressibility approach, the current improved primitive variable-based RPIM method is presently used to evaluate steady-state two-

dimensional laminar natural convection issues. The natural convection heat transfer in the annulus of concentric circular cylinders and the trapezoidal enclosures are used to demonstrate the capability and accuracy of the proposed method.

4.1. Natural Convection in the Annulus of Concentric Circular Cylinders

In this section, we simulate the natural convection heat transfer in a horizontal annulus of concentric circular cylinders at different temperatures using the RPIM model that was previously described. We selected this problem because, besides having curved boundaries and a wealth of experimental and numerical data available in the literature, it is a classical heat transfer problem that can be used to verify the accuracy of the current RPIM method.

In order to match the experimental conditions given in [24], we set the radius of the outer cylinder $r_o = 1.625$ and the inner one $r_i = 0.625$. The number of nodes, which are clustered near the walls to capture the boundary layer, is 161×25 for all simulations. The Prandtl number is 0.717, time step $\Delta t = 1$, and the fixed artificial compressibility factor equals 1×10^6, while the Rayleigh (Ra) numbers varied from 1×10^3 to 2.0×10^5. The temperature and velocity field are set to zero as the initial conditions. The inner cylinder is heated $\theta = 1$, and the outer cylinder is cooled $\theta = 0$ for the temperature boundary conditions. The Figure 2 shows the domain geometry, boundary conditions and the node distribution.

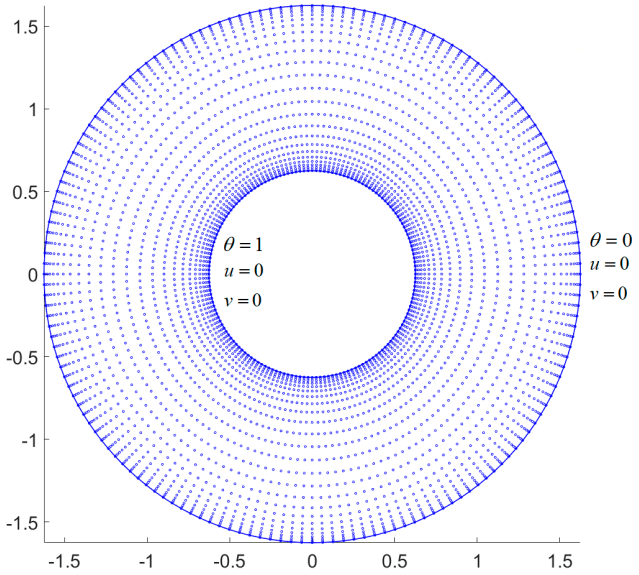

Figure 2. Annulus domain geometry, boundary conditions, and node distribution.

The temperature distribution obtained numerically is compared with the experimental temperature distributions from the interferograms under the same conditions (Figure 3). The left of Figure 3 is the isotherm plot obtained numerically. In contrast, the right of Figure 3 is an interferogram obtained experimentally. Within the cylinders, the fringes stand in for isotherms. Comparison of isotherm plots shows good agreement between numerical calculations and experimental results.

Figures 4–6 show the isothermal, and velocity fields, and stream function at steady state conditions for various $Ra = 2.38 \times 10^3$, 3.2×10^4, and 1.02×10^5. The buoyant force causes the fluid at the top of the inner cylinder to flow upwards and forms 2 symmetrical circulation eddies (Figures 4c, 5c and 6c). The Figures 4b, 5b and 6b show the flow direction and also indicate the thickness of the boundary layer. For low Ra number values, the speed of fluid movement is slow due to the influence of buoyancy, and the boundary layer also appears thick. The contribution of the convection term in the governing equations is weak, while the influence of the diffusion term is strong. As a result, the temperature distribution also resembles the distribution of conduction heat transfer. However, if Ra increases, the influence of the convection term becomes stronger, the flow of fluid movement becomes

faster, and the thickness of the boundary layer decreases. The (Figures 4b, 5b and 6b). This fast fluid movement also carries heat, so the temperature distribution is more even.

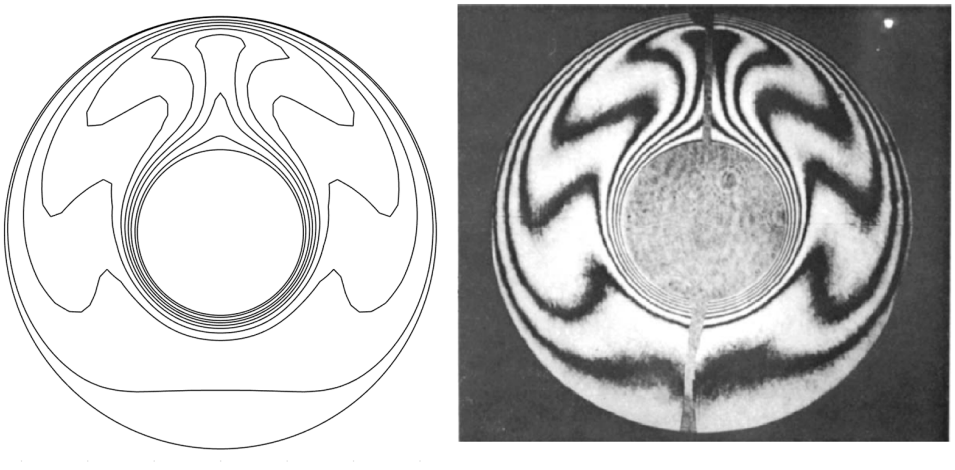

(**a**) (**b**)

Figure 3. Comparison of (**a**) numerical RPIM and (**b**) experimental isotherms [31] (with Permission) for $Ra = 4.7 \times 10^4$ and $Pr = 0.71$.

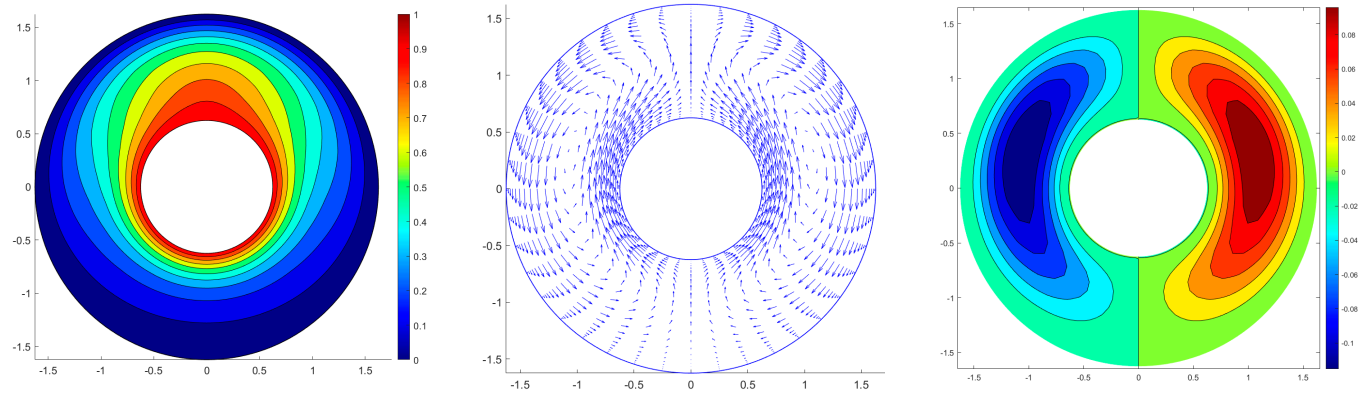

(**a**) (**b**) (**c**)

Figure 4. (**a**) Isotherm, (**b**) velocity fields, and (**c**) stream function of natural convection in circular annulus for $Ra = 2.38 \times 10^3$.

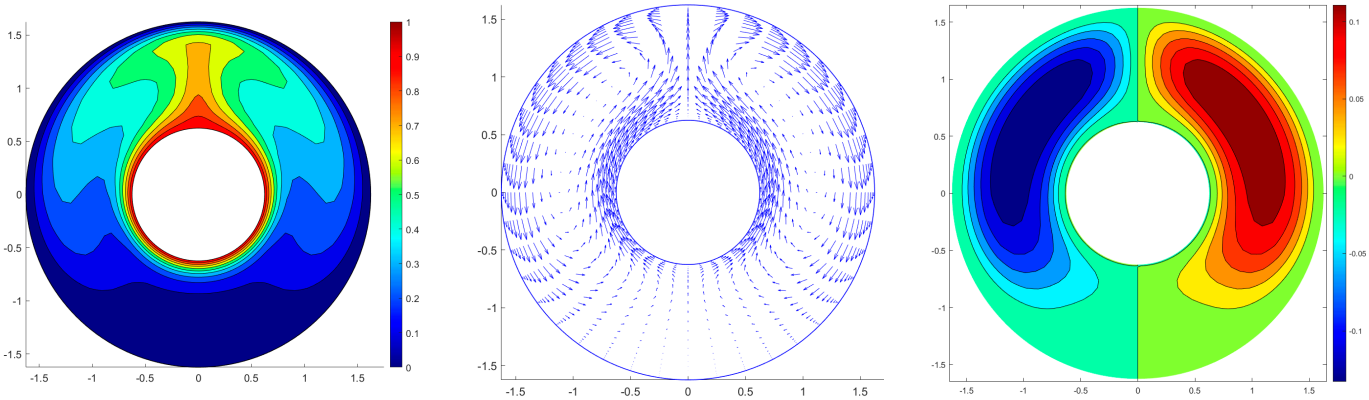

(**a**) (**b**) (**c**)

Figure 5. (**a**) Isotherm, (**b**) velocity fields, and (**c**) stream function of natural convection in circular annulus for $Ra = 3.2 \times 10^4$.

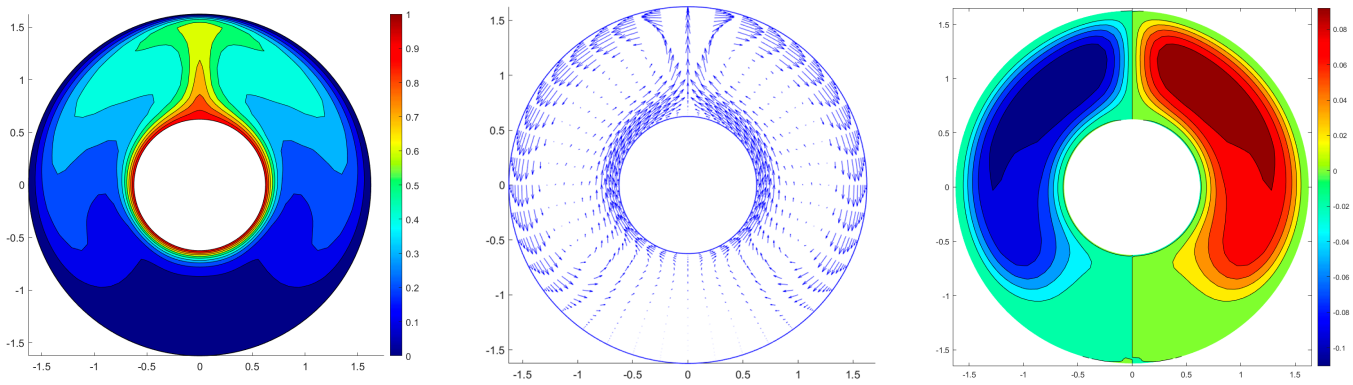

(**a**) (**b**) (**c**)

Figure 6. (**a**) Isotherm, (**b**) velocity fields, and (**c**) stream function of natural convection in circular annulus for $Ra = 1.02 \times 10^5$.

The average Nusselt number (Nu) for various Rayleigh numbers derived using the current RPIM method is compared with those experiments of Kuehn and Goldstein [32], Finite Difference Lattice Boltzmann method of Shi et al. [33], Discontinuous Galerkin method of Pranowo and Deendarlianto [34], and Galerkin Radial Basis Function of Ho-Minh et al. [35], Figure 7. The current results agree with the aforementioned references, as this figure illustrates.

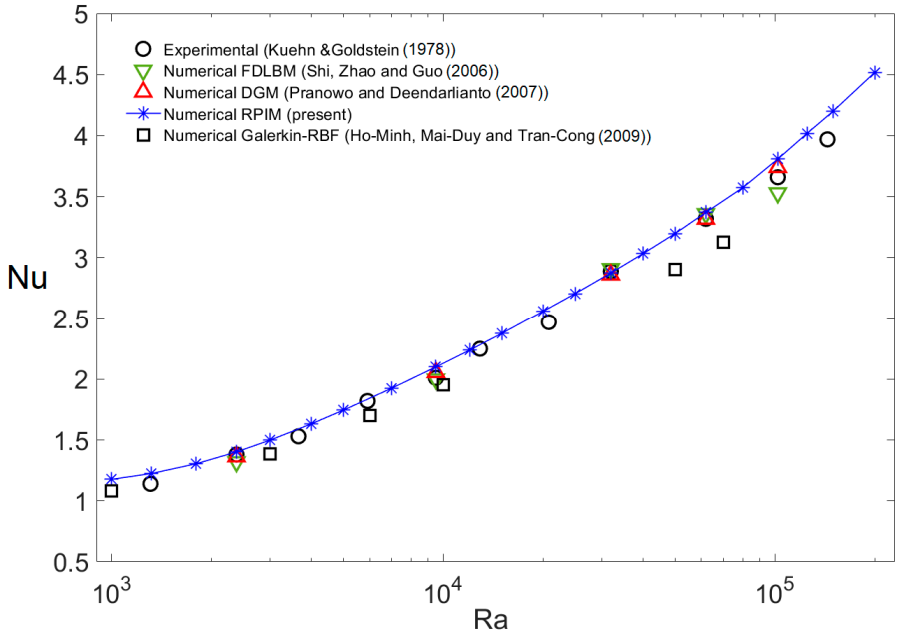

Figure 7. Comparison of average Nusselt number of natural convection in in circular annulus [32–35].

Based on Table 1, it can be seen that increasing the number of nodes produces a Nusselt number that is closer to the experimental results.

Table 1. The node convergence of the natural convection in the annulus for $Ra = 2.38 \times 10^3$.

Nodes	*Nu*	
	RPIM (Present Study)	Kuehn and Goldstein [32]
101 × 15	1.494	1.38
121 × 20	1.478	1.38
161 × 25	1.402	1.38

4.2. Natural Convection in a Trapezoidal Enclosure

The second test case, which involves natural convection in a trapezoidal enclosure for various Rayleigh numbers, is utilized to assess the proposed method. The short vertical wall's height (H) is the characteristic length, and the cavity length (L) is four times H. Meanwhile, the upper cavity's fixed inclination is 15 degrees. The boundary conditions are as follows: the left wall is heating, and the right wall is cooling [29]. The bottom and top walls are adiabatic walls. Meanwhile, the boundary condition for the velocity component at the wall is zero. For the values $Ra = 10^3$, 10^4, and $Ra = 10^5$, the shape parameter value is $C = 20$, and the number of nodes is 141×41. Meanwhile, for $Ra = 10^6$, the C value used is $C = 25$, and the number of nodes is 151×51. Figure 8 illustrates the geometry and the node distribution.

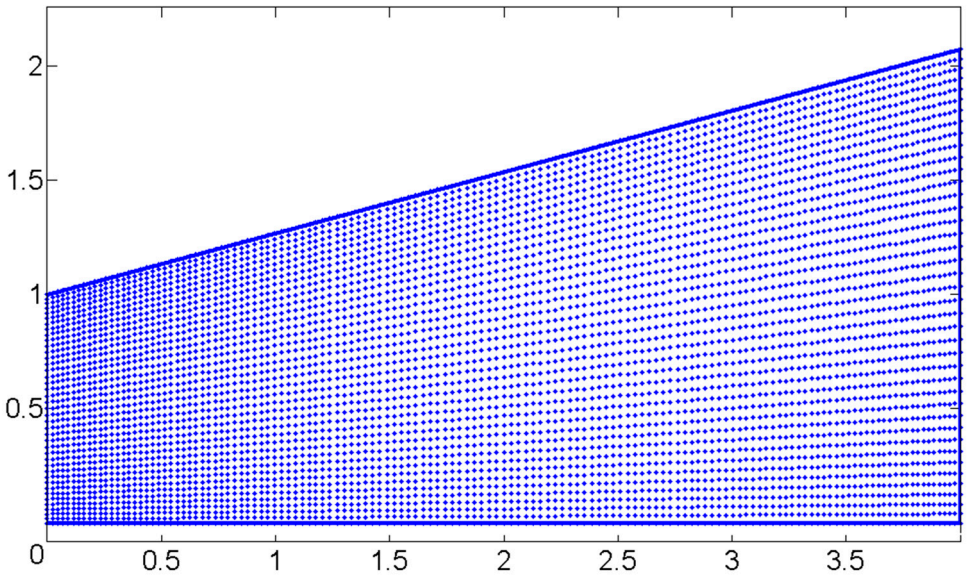

Figure 8. Trapezoidal domain geometry and node distribution.

The calculation results of natural convection in the trapezoidal enclosure are presented in the form of isothermal and stream functions. The airflow forms circulation, flowing up from the right due to the buoyant effect due to heating, then flowing to the left and down due to cooling, and finally flowing to the right. An increase in the Ra value causes the dominance of the convective term to strengthen and the speed to increase, so the isothermal forms a pattern that tends increasingly to the left at the top. Conversely, the isothermal tends increasingly to the right at the bottom (Figures 9a, 10a, 11a and 12a).

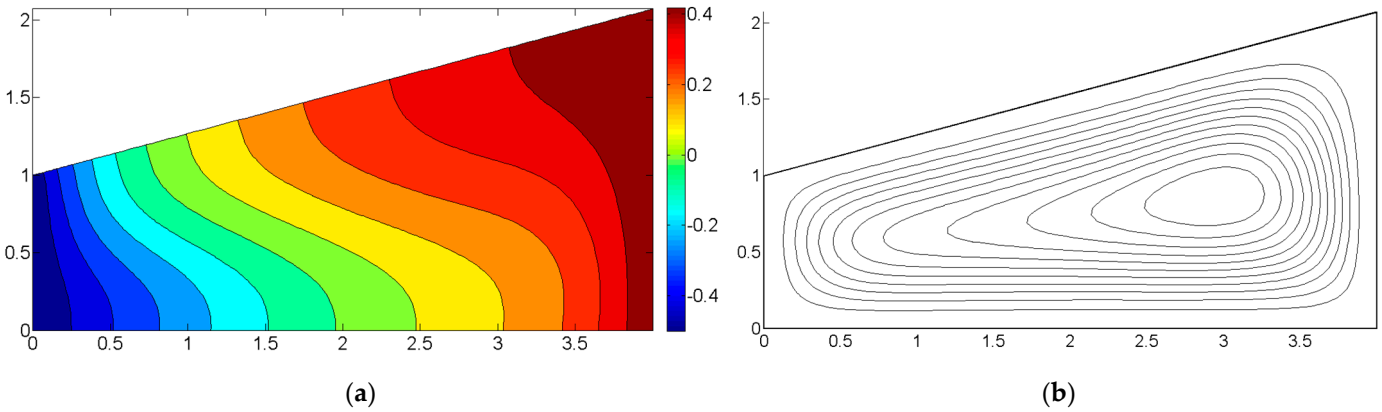

Figure 9. (**a**) Isotherm and (**b**) stream function of natural convection in trapezoidal cavity for $Ra = 10^3$.

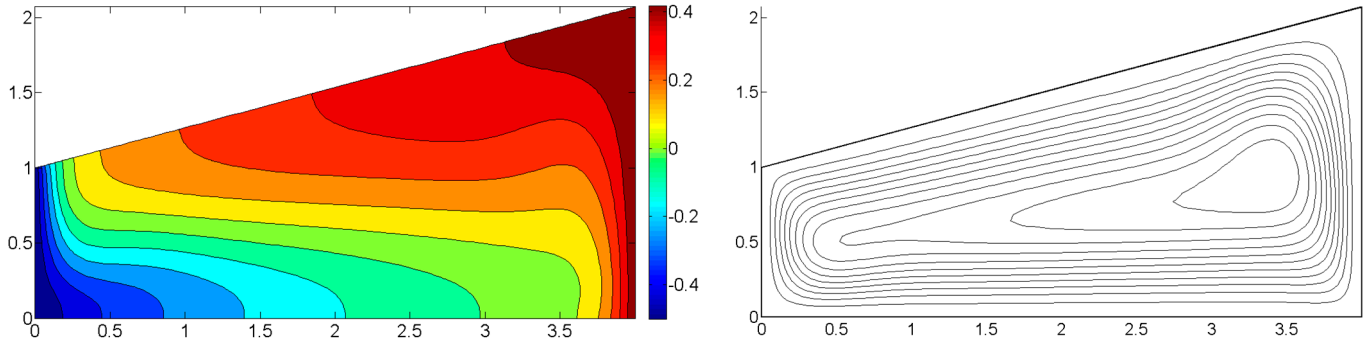

(**a**) (**b**)

Figure 10. (**a**) Isotherm and (**b**) stream function of natural convection in trapezoidal cavity for $Ra = 10^4$.

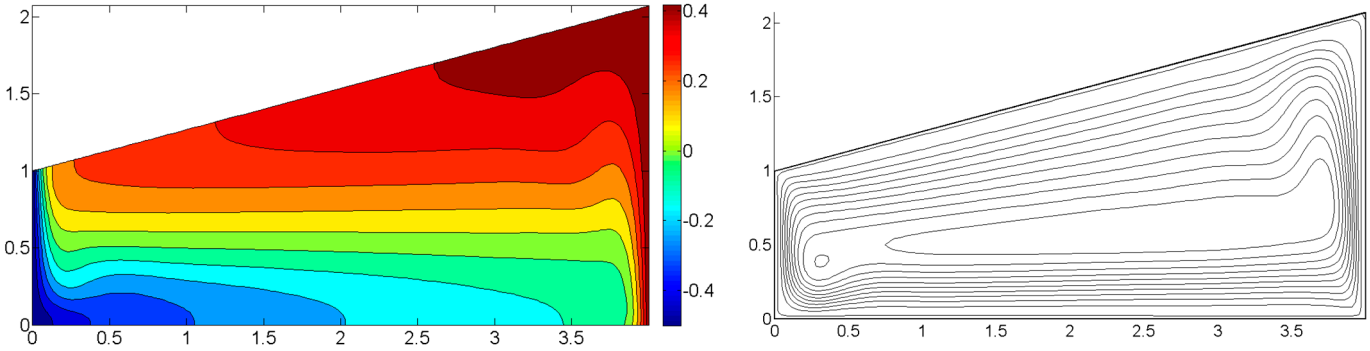

(**a**) (**b**)

Figure 11. (**a**) Isotherm and (**b**) stream function of natural convection in trapezoidal cavity for $Ra = 10^5$.

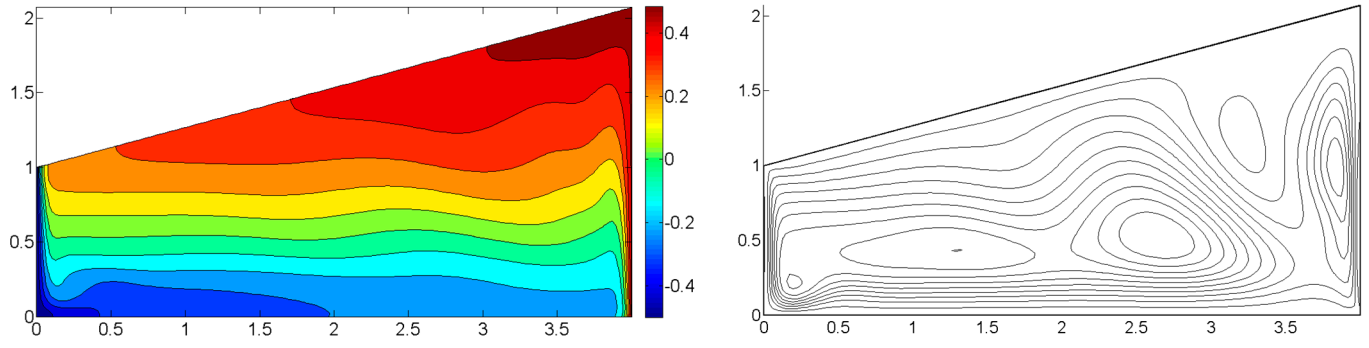

(**a**) (**b**)

Figure 12. (**a**) Isotherm and (**b**) stream function of natural convection in trapezoidal cavity for $Ra = 10^6$.

An increase in the Ra value causes the air circulation pattern to tend to slope because the speed increases (Figures 9b, 10b and 11b); apart from that, it also causes the calculation time to become longer to reach convergent conditions. This can be seen in Figure 13a–d. At the beginning of the calculation, the Nusselt number has a high value due to the effects of sudden heating and cooling, which then decreases and increases slightly. After reaching a steady state, the *Nu* value remains unchanged again. For the case of $Ra = 10^6$, the calculation until the pseudo time $t = 500$ is not enough. Steady conditions have not been reached; the flow pattern continues to change. This can be seen in Figure 12, where the flow circulation pattern should be gentle, but flow oscillations still occur.

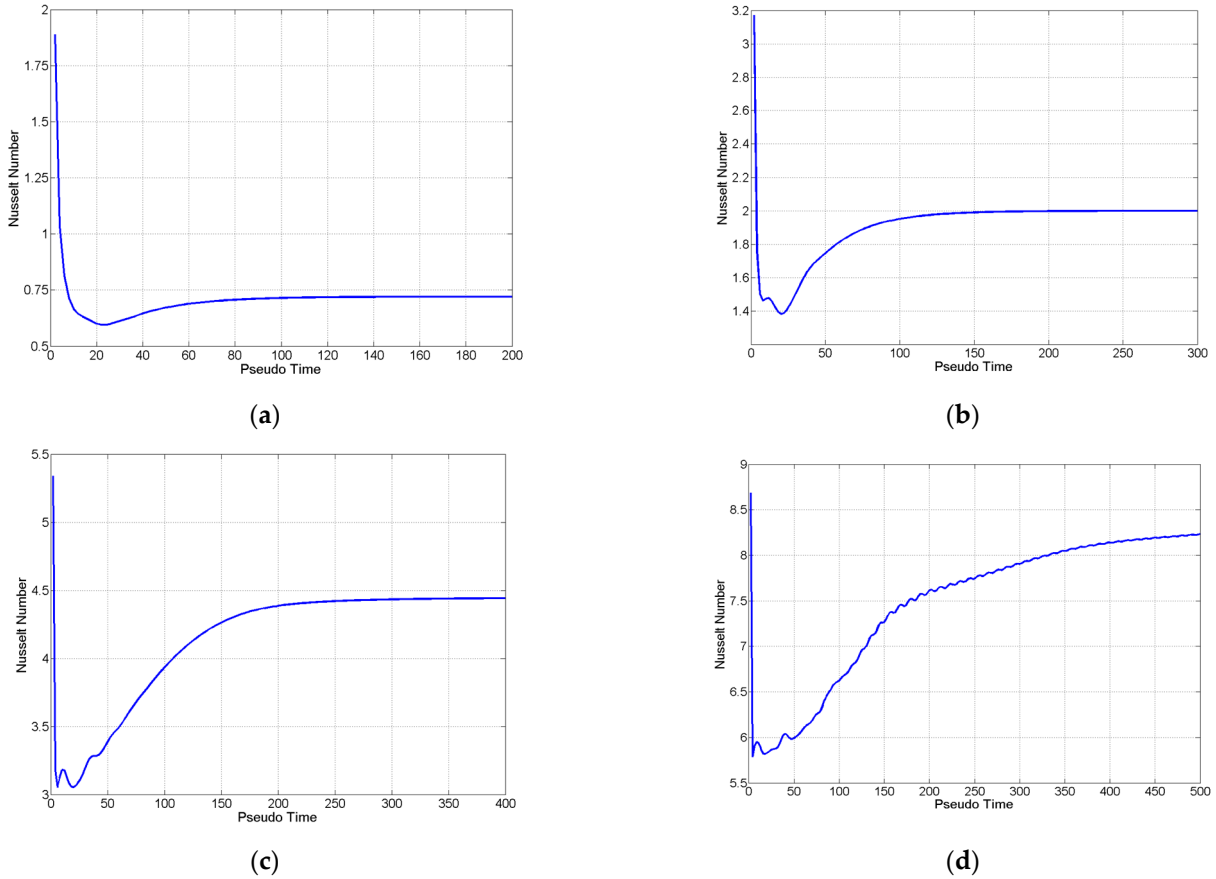

Figure 13. Convergent evolution of Nusselt numbers for (**a**) $Ra = 10^3$, (**b**) $Ra = 10^4$, (**c**) $Ra = 10^5$, (**d**) and $Ra = 10^6$.

The numerical calculation results of the RPIM method were compared with those of the numerical calculations of the Finite Volume method carried out by Moukalled and Darwish [36] to test the accuracy of the RPIM method. The results are presented in Table 2; the comparison shows good agreement.

Table 2. The comparison result of natural convection in trapezoidal enclosure other method results.

Ra	***Nu***	
	Moukalled and Darwish [36]	**RPIM (Present Study)**
10^3	0.6153	0.7205
10^4	1.9920	1.9993
10^5	4.4310	4.4419
10^6	8.8400	8.2320

5. Conclusions

This paper uses the artificial compressibility model and the RPIM method to solve the two-dimensional natural convection heat transfer problems. To assess the method's accuracy, two benchmark problems involving natural convection in the annulus of concentric circular cylinders and trapezoidal cavities are used as sample calculations. The suggested method's straightforward methodology makes solving natural convection in an irregular domain easy. There is also reasonable agreement when comparing the isotherms of the temperature fields of the RPIM in the annulus with the experimental interferogram. The proposed method's outstanding accuracy is demonstrated by comparison with solutions

from other numerical methods found in the literature, including the meshless Galerkin-RBF, Finite Difference Lattice Boltzmann (FDLBM), finite volume (FVM), and discontinuous Galerkin finite element (DGFEM) methods.

We plan to apply this technology in future studies to fuel cell modeling [37], two-phase thermofluid flow [38,39], and nanofluid simulation [40]. We also intend to employ parallel processing to accelerate the numerical calculating process.

Author Contributions: Conceptualization, P. and A.T.W.; methodology, P.; validation, P. and A.J.S.; formal analysis, P. and A.J.S.; investigation, P.; resources, A.T.W.; data curation, A.J.S.; writing—original draft preparation, P. and A.T.W.; writing—review and editing, P. and A.T.W.; supervision, A.T.W.; project administration, A.J.S. and A.T.W.; funding acquisition, A.T.W. All authors have read and agreed to the published version of the manuscript.

Funding: The financial support is provided by the Research Group of Sustainable Thermofluids, Universitas Sebelas Maret (through HGR UNS 2024 type A).

Data Availability Statement: No new data were created or analyzed in this study. Data sharing does not apply to this article.

Acknowledgments: Facilities provided by the Institute of Research and Community Service of Universitas Atma Jaya Yogyakarta and Universitas Sebelas Maret are acknowledged.

Conflicts of Interest: The authors declare no conflicts of interest.

References

1. Widyaparaga, A.; Pranowo. Simulation of conjugate convective-conductive heat transfer in a microchannel within the slip regime using GPU accelerated lattice Boltzmann method. In Proceedings of the ASME 2013 11th International Conference on Nanochannels, Microchannels, and Minichannels (ICNMM 2013), Sapporo, Japan, 16–19 June 2013. [CrossRef]
2. Mehrizi1, A.A.; Mohamad, A.A. Effect of the inclination angle and eccentricity on free convection heat transfer in elliptical–triangular annuli: A lattice Boltzmann approach. *Numer. Heat Transf. Part A* **2015**, *68*, 17–43. [CrossRef]
3. Couturier, H.; Sadat, S. Performance and Accuracy of a meshless method for laminar natural convection. *Numer. Heat Transf. Part B* **2000**, *37*, 455–467. [CrossRef]
4. Sophy, T.; Sadat, H.; Prax, C. A meshless formulation for three-dimensional laminar natural convection. *Numer. Heat Transf. Part B* **2002**, *41*, 433–445. [CrossRef]
5. Liu, G.R.; Wu, Y.L. Application of meshless point interpolation method with matrix triangularization algorithm to natural convection. In Proceedings of the 1st Asian Workshop on Meshfree Methods—Advances in Meshfree and X-FEM Methods Advances in Meshfree and X-FEM Methods, Singapore, 16–18 December 2002. [CrossRef]
6. Wijayanta, A.T.; Pranowo. A localized meshless approach using radial basis functions for conjugate heat transfer problems in a heat exchanger. *Int. J. Refrig.* **2020**, *110*, 38–46. [CrossRef]
7. Lu, Y.Y.; Belytschko, T.; Tabbara, M. Element-free Galerkin method for wave propagation and dynamic fracture. *Comput. Methods Appl. Mech. Eng.* **1996**, *126*, 131–153. [CrossRef]
8. Belytschko, T.; Tabbara, M. Dynamic fracture using Element-free Galerkin methods. *Int. J. Numer. Methods Eng.* **1996**, *39*, 923–938. [CrossRef]
9. Manzin, A.; Bottauscio, O. Element-free Galerkin method for the analysis of electromagnetic-wave scattering. *IEEE Trans. Magn.* **2008**, *44*, 1366–1369. [CrossRef]
10. Singh, A.; Singh, I.V.; Prakash, R. Meshless element free Galerkin method for unsteady nonlinear heat transfer problems. *Int. J. Heat Mass Transf.* **2007**, *50*, 1212–1219. [CrossRef]
11. Singh, I.V.; Jain, P.K. Parallel meshless EFG solution for fluid flow problems. *Numer. Heat Transf. Part B* **2005**, *48*, 45–66. [CrossRef]
12. Vlastelica, I.; Isailović, V.; Djukić, T.; Filipović, N.; Kojić, M. On accuracy of the element-free Galerkin (EFG) method in modeling incompressible fluid flow. *J. Serb. Soc. Comput. Mech.* **2008**, *2*, 90–99.
13. Zhang, X.; Zhang, P. Numerical Modeling of Stokes Flow in a Circular Cavity by Variational Multiscale Element Free Galerkin Method. *Math. Probl. Eng.* **2014**, *2014*, 451546. [CrossRef]
14. Zhang, L.; Ouyang, J.; Zhang, X.H. On a two-level element-free Galerkin method for incompressible fluid flow. *Appl. Numer. Math.* **2009**, *59*, 1894–1904. [CrossRef]
15. Zhang, X.; Zhang, P. Meshless modeling of natural convection problems in non-rectangular cavity using the variational multiscale element free Galerkin method. *Eng. Anal. Bound. Elem.* **2015**, *61*, 287–300. [CrossRef]
16. Wu, Y.L.; Liu, G.R.; Gu, Y.T. Application of meshless local Petrov-Galerkin (MLPG)approach to simulation of incompressible flow. *Numer. Heat Transfer. Part B* **2005**, *48*, 459–475. [CrossRef]
17. Arefmanesh, A.; Najafi, M.; Nikfar, M. Meshless Petrov–Galerkin simulation of buoyancy-driven fluid flow and heat transfer in a cavity with wavy side walls. *CMES-Comput. Model. Eng. Sci.* **2010**, *62*, 113–149. [CrossRef]

18. Arefmanesh, A.; Najafi, M.; Abdi, H. Meshless local Petrov-Galerkin method with unity test function for non-isothermal fluid flow. *CMES-Comput. Model Eng. Sci.* **2008**, *25*, 9–22. [CrossRef]
19. Avila, R.; Atluri, S.N. Numerical solution of non-steady flows, around surfaces in spatially and temporally arbitrary motions, by using the MLPG method. *CMES-Comput Model Eng. Sci.* **2009**, *54*, 15–64. [CrossRef]
20. Najafi, M.; Arefmanesh, A.; Enjilela, V. Extending MLPG primitive variable-based method for implementation in fluid flow and natural, forced and mixed convection heat transfer. *Eng. Anal. Bound. Elem.* **2013**, *37*, 1285–1299. [CrossRef]
21. Najafi, M.; Enjilela, V. Natural convection heat transfer at high Rayleigh numbers—Extended meshless local Petrov–Galerkin (MLPG) primitive variable method. *Eng. Anal. Bound. Elem.* **2014**, *44*, 170–184. [CrossRef]
22. Liu, G.R.; Zhang, G.Y.; Gu, Y.T.; Wang, Y.Y. A meshfree radial point interpolation method (RPIM) for three-dimensional solids. *Comput. Mech.* **2005**, *36*, 421–430. [CrossRef]
23. Le Quere, P. Accurate solutions to the square thermally driven cavity at high Rayleigh number. *Comput. Fluids* **1991**, *20*, 29–41. [CrossRef]
24. Cui, X.Y.; Liu, G.R.; Li, G.Y.; Zhang, G.Y. A thin plate formulation without rotation DOFs based on the radial point interpolation method and triangular cells. *Int. J. Numer. Methods Eng.* **2010**, *85*, 958–986. [CrossRef]
25. Chorin, A.J. A numerical method for solving incompressible viscous flow problems. *J. Comput. Phys.* **1967**, *2*, 12–26. [CrossRef]
26. Nithiarasu, P.; Liu, C.B. Steady and unsteady incompressible flow in a double driven cavity using the artificial compressibility (AC)-based characteristic-based split (CBS) scheme. *Int. J. Numer. Methods Eng.* **2005**, *63*, 380–397. [CrossRef]
27. Nithiarasu, P. An efficient artificial compressibility (AC) scheme based on the characteristic based split (CBS) method for incompressible flows. *Int. J. Numer. Methods Eng.* **2003**, *56*, 1815–1845. [CrossRef]
28. Malan, A.G.; Lewis, R.W.; Nithiarasu, P. An improved unsteady, unstructured, artificial compressibility, finite volume scheme for viscous incompressible flows: Part I. Theory and implementation. *Int. J. Numer. Methods Eng.* **2002**, *54*, 695–714. [CrossRef]
29. Manzari, M.T. An explicit finite element algorithm for convection heat transfer problems. *Int. J. Numer. Methods Heat Fluid Flow* **1999**, *9*, 860–877. [CrossRef]
30. Pranowo; Wijayanta, A.T. Numerical solution strategy for natural convection problems in a triangular cavity using a direct meshless local Petrov-Galerkin method combined with an implicit artificial-compressibility model. *Eng. Anal. Bound. Elem.* **2021**, *126*, 13–29. [CrossRef]
31. Kuehn, T.H.; Goldstein, R.J. An experimental and theoretical study of natural convection in the annulus between horizontal concentric cylinders. *J. Fluid Mech.* **1976**, *74*, 695–719. [CrossRef]
32. Kuehn, T.H.; Goldstein, R.J. An Experimental Study of Natural Convection Heat Transfer in Concentric and Eccentric Horizontal Cylindrical Annuli. *J. Heat Transf.* **1978**, *100*, 635–640. [CrossRef]
33. Shi, Y.; Zhao, T.S.; Guo, Z.L. Finite difference-based lattice Boltzmann simulation of natural convection heat transfer in a horizontal concentric annulus. *Comput. Fluids* **2006**, *35*, 1–15. [CrossRef]
34. Pranowo; Deendarlianto. Numerical solution of steady-state free convection using unstructured discontinuous Galerkin method. In Proceedings of the 3rd International Conference on Product Design & Development 2007, Yogyakarta, Indonesia, 12 December 2007.
35. Ho-Minh, D.; Duy-Mai, N.; Tran-Cong, T. A Galerkin-RBF approach for the streamfunction-vorticity-temperature formulation of natural convection in 2D enclosured domains. *CMES-Comput. Model. Eng. Sci.* **2009**, *44*, 219–248. [CrossRef]
36. Moukalled, F.; Darwish, M. Natural convection in a trapezoidal enclosure heated from the side with a baffle mounted on its upper inclined surface. *Heat Transf. Eng.* **2004**, *25*, 80–93. [CrossRef]
37. Hosseini, V.R.; Mehrizi, A.A.; Karimi-Maleh, H.; Naddafi, M. A numerical solution of fractional reaction–convection–diffusion for modeling PEM fuel cells based on a meshless approach. *Eng. Anal. Bound. Elem.* **2023**, *155*, 707–716. [CrossRef]
38. Enoki, K.; Ono, M.; Okawa, T.; Akisawa, A.; Mori, H.; Kristiawan, B.; Wijayanta, A.T. Two-phase flow regimes of refrigerant R134a in an oscillating horizontal rectangular minichannel conduit. *Int. J. Refrig.* **2020**, *118*, 261–268. [CrossRef]
39. Pranowo; Wijayanta, A.T.; Itaya, Y. Numerical simulation of coalescence and break-up of drops in shear flow based on the meshless localized radial basis function method. In Proceedings of the 10th International Conference on Physics and Its Applications (ICOPIA 2020), Surakarta, Indonesia, 26 August 2020. [CrossRef]
40. Kristiawan, B.; Wijayanta, A.T.; Enoki, K.; Miyazaki, T.; Aziz, M. Heat transfer enhancement of TiO_2/water nanofluids flowing inside a square minichannel with a microfin structure: A numerical investigation. *Energies* **2019**, *12*, 3041. [CrossRef]

Disclaimer/Publisher's Note: The statements, opinions and data contained in all publications are solely those of the individual author(s) and contributor(s) and not of MDPI and/or the editor(s). MDPI and/or the editor(s) disclaim responsibility for any injury to people or property resulting from any ideas, methods, instructions or products referred to in the content.